Modeling aspects and Gain scheduled H_∞ Controller Design for an Electrostatic micro-Actuator with Squeezed Gas Film Damping Effects

Marialena Vagia and Anthony Tzes

Abstract— In this article the modeling and control design aspects of an electrostatic microactuator (EmA) with squeezed thin film damping effects are presented. The modeling analysis of the squeezed film damping effect is investigated in the case of an EmA composed by a set of two plates. The bottom plate is clamped to the ground, while the moving plate is driven by an electrically induced force which is opposed by the force exerted by a spring element. The nonlinear model of the EmA is linearized at various operating points, and the feedforward compensator provides the nominal voltage. Subsequently a gain scheduled H_∞ controller is used to tune the controller-parameters depending on the EmA's operating conditions. The controller is designed at various operating points based on the distance between its plates. The parameters of the controller are tuned in an optimal manner and computed via the use of the Linear Matrix Inequalities. Special attention is paid in order to examine the stability issue in the intervals between the operating points. Simulation results investigate the efficacy of the suggested modeling and control techniques.

I. INTRODUCTION

With the rapid progress of micro and nano fabrication processes in the recent years it is now possible to fabricate miniaturized devices whose size varies from micro to nano scales [1]. The focus is on creating high performance devices which are sensitive and have high quality factor [2], [3]. The dynamic behavior of movable parts in MEMS is largely affected by the supporting environmental conditions such as the air pressure, temperature et. al. This gas-structure inter-action [4] has been encountered in certain devices such as accelerometers, gyroscopes and RF-switches [5], [6] which are designed to operate in rarified air condition, whereas other devices, such as microphones, ultrasonic transducers and micro mirrors, generally work with ambient air surround-ing them. Therefore, the effects of the surrounding air and most notably the damping force which can be neglected in structures of conventional dimensions, play a critical role with micro-structures with diminutive size [7].

Squeezed film damping is a term used to describe the most common fluid-structure interaction that impacts the performance of MEMS devices. Squeezed film damping occurs when a thin film layer of air or some other fluid separating the free structure from the substrate is "squeezed" due to any possible movement of the free structure normal to the substrate. Silicon microstructures (sensors and actuators) that make use of the capacitive measurement principles [8], or electrostatic driving forces [9], are characterized by very small gaps between their moving surfaces [5] and so the dynamic behavior of movable parts in these electrostatic actuators is largely affected by the air's presence (i.e. low

The authors are with the Electrical and Computer Engineering De-partment, University of Patras, Rio, Achaia-26500, Greece. Corresponding author's e-mail: mvagia@ece.upatras.gr

vacuum conditions for micro-accelerometers [10], ultra thin gas film in magnetic/disk interfaces [11] and tilting micro-mirrors in DLP type projectors [12], [13]). The understanding of the squeeze film damping mechanism in such electrostatic micro-actuator (EmA) devices [14] is necessary in order to optimize the controller designs.

The inclusion of the squeeze film damping effects in-creases the complexity of the dynamics of the micro actuator plant [15], [16], and appropriate controllers should deal with it [17]. Accordingly, since these systems are highly non-linear and have a large order, the tendency is to design controllers that are based on linearized models of the system [13].

In the present article a Gain Scheduled H_∞ controller [18], [19] is designed for a class of Linear Parameter Varying (LPV) plants characterizing the EmA. The main idea is to separate the control design process into two steps. Firstly the local linear controllers are designed based on the linearizations of the nonlinear system at several operating points [20]. In the sequel, a global controller for the nonlinear plant is obtained by interpolating or scheduling the gains of the local operating points design. The linearized plants' state space matrices are assumed to depend on a vector of spatial varying parameters. The measured parameters, are fed to the controller to optimize the performance and the robustness of the closed loop system. The resulting controller is auto-matically "gain scheduled" along parameter trajectories. The synthesis problem of the controller is fulfilled with the use of the Linear Matrix Inequalities (LMIs).

In the rest of this article the modeling of the EmA with squeezed film damping effects is presented in Section II. In Section III the design of the Gain scheduled H_∞ con-trol scheme is presented. Simulation results that prove the efficacy of the proposed control architecture are presented in Section IV, while the conclusions are drawn in the last Section V.

II. MODELING OF PARALLEL PLATE ACTUATORS WITH SQUEEZE AIR DAMPING

The EmA from a structural point of view corresponds to a micro–capacitor whose one plate is attached to the ground while its other moving plate is floating on the air [21], [22], [23] with the aid of an additional external spring. Figure 1 presents the structure of the EmA. The dynamic nonlinear governing equation of the system [2] is:

$$m\ddot{\eta} + F_d + k\eta = \frac{\varepsilon \ell U^2}{2(\eta^{\max} - \eta)^2} = F_{el} \qquad (1)$$

where η is the displacement of the plates from the relaxed position, m is the plate's mass, k is the spring's stiffness, ℓ is the length of the square plate, U is the applied voltage

between the capacitor's plates, $\eta^{\max}$ is the distance of the plates when the spring is relaxed, ε is the dielectric constant of the air, F_d is the force caused by the parallel plate damper and F_{el} is the electrically-induced force as shown in Figure 2.
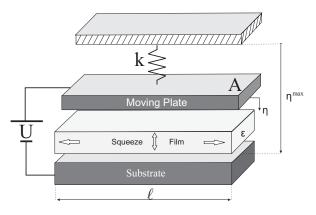

Fig. 1.   Electrostatic micro–Actuator structure

A. Electrical Force Model

Application of a voltage U between the capacitor's plates generates an electrically–induced force [24], [25]

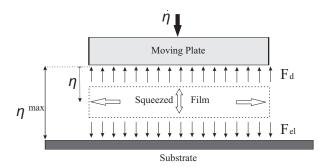$$F_{el} = \frac{\varepsilon \ell^2 U^2}{2(\eta^{\max} - \eta)^2}.$$ (2)

Fig. 2.   Diagram of forces applied on the μ-A

B. Squeezed Film Damping Effect

The behavior of the gas between the plates is in general governed by both viscous and inertial effect within the fluid. However for the very small dimensions encountered in electrostatic devices, the inertial effect is often negligible. In such a case, the behavior of the fluid is governed by the Reynolds equation, a single expression which relates pressure, density and surface velocity for the specific geometry of a bounded film [4], [15], [26], [27].

Under the assumption of isothermal conditions, Blench [28] has derived solutions for the pressure between the gap of two oscillating rectangular plates. The pressure has two components, one in phase with the drive, which represents the spring-like behavior of the gas, and one in phase with the velocity which represents the damping behavior [15]. The integrals of these pressures over the plates provides the expressions for the air spring and damping contributions. For square plates [15], [28] the coefficient of the viscous damping

force due to the squeezed film air damping is [29], [30], [31] (under the assumption of a sinusoidal motion of the upper plate with frequency ω):

$$b_1(\eta,\omega) = \frac{64\sigma P_a \ell^2}{\omega \pi^6 (\eta^{\max} - \eta)} \sum_{m,n \text{ odd}} \frac{m^2 + n^2}{(mn)^2 \{[m^2 + n^2]^2 + \sigma^2/\pi^4\}}$$

and the coefficient of elastic damping force is:

$$k_1(\eta,\omega) = \frac{64\sigma^2 P_a \ell^2}{\pi^8 (\eta^{\max} - \eta)} \sum_{m,n \text{ odd}} \frac{1}{(mn)^2 \{[m^2 + n^2]^2 + \sigma^2/\pi^4\}}$$

where $\sigma = \frac{12\mu \ell^2 \omega}{P_a(\eta^{\max} - \eta)}$ is the dimensionless squeeze number, P_a is the ambient pressure, and μ is the (air) viscocity coefficient. It should be noticed that for typical gaps encountered in EmAs (0.1μm $\leq \eta^{\max} - \eta \leq 40\mu$m) over an operating frequency range of less than $\omega^{\max} = 100$MHz, the coefficient k_1 increases with the frequency and is significantly smaller than k, ($k_1 \ll k$, $\forall \omega \in [0, \omega^{\max})$). The force caused by the parallel plate damper F_d presented in equation (1) is equal to [32]:

$$F_d = b_1(\eta,\omega)\dot{\eta} + k_1(\eta,\omega)\eta.$$ (3)

C. Linearized Equations of Motion

The nonlinear equation of motion for (1) can be rewritten according to (3):

$$m\ddot{\eta} + b_1(\eta,\omega)\dot{\eta} + (k + k_1(\eta,\omega))\eta = \frac{\varepsilon \ell^2 U^2}{2(\eta^{\max} - \eta)^2}.$$ (4)

Equation (4) is a nonlinear equation due to the presence of ω, η, U. A model approximation can be obtained if a certain operating point $\dot{\eta}_i^\circ$, η_i°, ω° is chosen in order to achieve a linearized system. All possible "equilibria"-points η_i°, $i = 1, \ldots, M$ depend on the applied nominal voltage U_i°. Equation (4) for $\omega^\circ \simeq 0, \dot{\eta}_i^\circ = 0, \eta_i^\circ$ yields

$$\left(k + k_1 \big|_{\eta = \eta_i^\circ, \omega^\circ \simeq 0} \right) \eta_i^\circ = k\eta_i^\circ = \frac{\varepsilon \ell^2 (U_i^\circ)^2}{2(\eta^{\max} - \eta_i^\circ)^2}, \text{or}$$ (5)

$$U_i^\circ = \pm \left[\frac{2k\eta_i^\circ (\eta^{\max} - \eta_i^\circ)^2}{\varepsilon \ell^2} \right]^{1/2}.$$ (6)

This nominal U_i°–voltage must be applied if the capacitor's plate is to be maintained at a certain distance η_i° from its un–stretched position

If the above system is linearized with respect to the parameter η, and if ω is equal to a certain value (i.e. ω°) the approximated linearized equations of motion around the equilibria points (U_i°, η_i°, and $\dot{\eta}_i^\circ = 0$) can be found using standard perturbation theory for the variables U and η_i where $U = U_i^\circ + \delta u$ and $\eta_i = \eta_i^\circ + \delta \eta_i$. The linearized equation of motion for the system in (4) is:

$$m\delta\ddot{\eta}_i + \left(b_1 \big|_{\eta = \eta_i^\circ, \omega = \omega^\circ} \delta\dot{\eta}_i \right) + \left(k + k_1 \big|_{\eta = \eta_i^\circ, \omega = \omega^\circ} + \frac{\vartheta k_1}{\vartheta \eta} \big|_{\eta = \eta_i^\circ, \omega = \omega^\circ} \eta_i^\circ \right) \delta\eta_i$$

$$+ \left(k + k_1 \big|_{\eta = \eta_i^\circ, \omega = \omega^\circ} \right) \eta_i^\circ$$

$$= \frac{\varepsilon \ell^2 (U_i^\circ)^2}{2(\eta^{\max} - \eta_i^\circ)^2} + \frac{\varepsilon \ell^2 (U_i^\circ)^2}{(\eta^{\max} - \eta_i^\circ)^3} \delta\eta_i + \frac{\varepsilon \ell^2 U_i^\circ}{(\eta^{\max} - \eta_i^\circ)^2} \delta u$$

Since

$\left(k+k_1\big|_{\eta=\eta_i^\circ,\omega=\omega^\circ}\right)\simeq k$, and after the substitution of:

$$k_i^a = k+k_1\big|_{\eta=\eta_i^\circ,\omega=\omega^\circ}+\frac{\vartheta k_1}{\vartheta\eta}\big|_{\eta=\eta_i^\circ,\omega=\omega^\circ}\eta_i^\circ-\frac{\varepsilon\ell^2(U_i^\circ)^2}{(\eta^{\max}-\eta_i)^3},$$

$$b_i = b_1\big|_{\eta=\eta_i^\circ,\omega=\omega^\circ}, \qquad \beta_i=\frac{\varepsilon\ell^2 U_i^\circ}{(\eta^{\max}-\eta_i^\circ)^2}, \quad i=1,\ldots,M$$

Equation (7) is transformed to:

$$m\delta\ddot{\eta}_i+b_i\delta\dot{\eta}_i+k_i^a\delta\eta_i=\beta_i\delta u. \tag{7}$$

Equation (7) is valid only for a specific frequency ω°, and therefore the characterization of the system's behavior over a frequency range $\omega\in[0,\omega^{\max})$ can be investigated by examining these equations for a vector of frequencies $\omega^{\circ,j}$, $j=1,\ldots,N$ spanning this interval. Having obtained the frequency response of the system for a given operating point η_i° this is approximated by an nth order approximation. It should be noted that a second order approximation suffices for the description of the linearized EmA-dynamics. This second order approximation yields to a state space description equal to:

$$\left[\begin{array}{c}\delta\dot{\tilde{\eta}}_i\\\delta\ddot{\tilde{\eta}}_i\end{array}\right] = \left[\begin{array}{cc}0 & 1\\a_{21}(\eta_i^\circ) & a_{22}(\eta_i^\circ)\end{array}\right]\left[\begin{array}{c}\delta\tilde{\eta}_i\\\delta\dot{\tilde{\eta}}_i\end{array}\right]+\left[\begin{array}{c}0\\1\end{array}\right]\delta u$$

$$= A_i(\eta_i^\circ)\left[\begin{array}{c}\delta\tilde{\eta}_i\\\delta\dot{\tilde{\eta}}_i\end{array}\right]+B\delta u, \quad i=1,\ldots,M \tag{8}$$

$$\delta\eta_i = [c_{11}(\eta_i^\circ)\ \ c_{12}(\eta_i^\circ)]\left[\begin{array}{c}\delta\tilde{\eta}_i\\\delta\dot{\tilde{\eta}}_i\end{array}\right]=C(\eta_i^\circ)\left[\begin{array}{c}\delta\tilde{\eta}_i\\\delta\dot{\tilde{\eta}}_i\end{array}\right],$$

where $[\delta\tilde{\eta}_i,\delta\dot{\tilde{\eta}}_i]^T$ is a vector obtained from a similarity transformation (controller canonical form) with respect to the the the vector $[\delta\eta,\delta\dot{\eta}_i]^T$.

III. GAIN SCHEDULED H_∞ CONTROLLER DESIGN

The feedback term is a gain scheduled H_∞ controller, which consists of an LTI controller for each one of aforementioned subsystems. These controllers switch among them when the operating conditions change. The change of the system matrices depends on the variation of the operating point η_i. The designed controller is applied to the nonlinear system of the EmA in order to test its efficacy. The controller's parameters are tuned with the use of LMIs [33], [34].

In order to appropriately weight selected frequency bounds under consideration, the system's input and output are filtered by filters of transfer functions $W_1(s),W_2(s)$. For the EmA, the low frequency spectrum is of primary importance and low pass filters $W_1(s)=\prod_{i=1}^q\frac{w_{1,i}}{s+w_{1,i}},W_2(s)=\prod_{j=1}^f\frac{w_{2,j}}{s+w_{2,j}}$ are used throughout this frequency-shaping procedure. In the sequel, driven by our application (micropositioning) first order (q,f=1) low pass filters are used. The linearized system's description using the augmented state vector $\delta\eta_i^a=[\delta\tilde{\eta}_i,\delta\dot{\tilde{\eta}}_i,\eta_f]^T$ together with the other filter is equal to:

$$\left[\begin{array}{c}\delta\dot{\tilde{\eta}}_i\\\delta\ddot{\tilde{\eta}}_i\\\dot{\eta}_f\\\hline\dot{\eta}_q\\\hline\delta\bar{\eta}_i\end{array}\right]=\left[\begin{array}{ccc|c|c}0 & 1 & 0 & 0 & 0\\a_{21} & a_{22} & 0 & 0 & b_{21}\\w_{2,1}c_{11} & w_{2,1}c_{12} & -w_{2,1} & 0 & 0\\\hline -w_{1,1}c_{11} & -w_{1,1}c_{12} & 0 & -w_{1,1} & w_{1,1}\\\hline 1 & 0 & 0 & 0 & 0\end{array}\right]\left[\begin{array}{c}\delta\tilde{\eta}_i\\\delta\dot{\tilde{\eta}}_i\\\eta_f\\\hline\eta_q\\\hline\delta u\end{array}\right]$$

$$=\left[\begin{array}{c|c|c}A_i^a & B_1^a & B_i^a\\\hline c_{1,i}^a & D_{11} & D_{12}\\\hline c^a & D_{21} & D_{22}\end{array}\right]\left[\begin{array}{c}\delta\tilde{\eta}_i\\\delta\dot{\tilde{\eta}}_i\\\eta_f\\\hline\eta_q\\\hline\delta u\end{array}\right] \tag{9}$$

For the a priori selected operating points η_i°, the system's description is within the convex hull of the matrices:

$$\left[\begin{array}{cc}A_i^a(\eta_i) & B_i^a(\eta_i)\\C^a & 0\end{array}\right]\in\text{Co}\left\{\left[\begin{array}{cc}A_i^a(\eta_i^o) & B_i^a(\eta_i^o)\\C^a & 0\end{array}\right],i=1,\ldots,M\right\}$$

Under the assumption of direct measurements of the state vector $\delta\eta_i^a$ the controller adjusts in a gain scheduled approach its parameters based on the neighborhood of the selected operating point η_i°.

In this scheme, the plate's gap space $\eta\in[\eta^{\min},\eta^{\max})$ is equidistantly divided into n-segments, where defined by the selected operating points:

$$\eta_i^\circ=\eta^{\min}+(i-1)\frac{\eta^{\max}-\eta^{\min}}{n}=\eta_i^\circ=\eta_i^{\min}+(i-1)\Delta,$$
$$i=1,\ldots,n \tag{10}$$

When $\eta_i\in[\eta_i^\circ-\frac{\Delta}{2},\eta_i^\circ+\frac{\Delta}{2})$ the $\delta\eta_i^a$ are computed with respect to the ith operating point. The gain-scheduled controller provides a dynamic feedback of the form

$$\delta u=K(s,\eta_i)\delta\eta_i^a\ , \tag{11}$$

where with a slight abuse of notation, we imply that the $K(s)$–transfer function depends on the operating point η_i, noted as $K(s,\eta_i)$.

The architecture of the control scheme is presented in Figure 3 [35]:
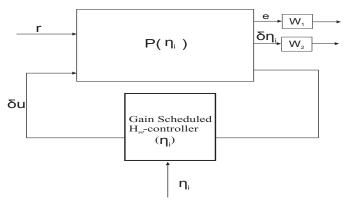

Fig. 3. Controller Architecture

The goal is to create a controller with a form:

$$\dot{x}_c=A_c(\eta_i)x_c+B_c(\eta_i)\delta\eta_i^a$$
$$\delta u=C_c(\eta_i)x_c+D_c(\eta_i)\delta\eta_i^a \tag{12}$$

that guarantees a quadratic H_∞ performance less than γ for the closed loop system, where $x_c\in R^k$ is the state vector of the controller. With the notation

$$\Omega(\eta_i):=\left[\begin{array}{cc}A_c(\eta_i) & B_c(\eta_i)\\C_c(\eta_i) & D_c(\eta_i)\end{array}\right] \tag{13}$$

the state space matrices of the closed loop system are:

$$A_{cl}(\eta_i)=A_o(\eta_i)+\mathscr{B}\Omega(\eta_i)\mathscr{C}$$
$$B_{cl}(\eta_i)=B_o(\eta_i)+\mathscr{B}\Omega(\eta_i)\mathscr{D}_{21}$$
$$C_{cl}(\eta_i)=C_o(\eta_i)+\mathscr{D}_{12}\Omega(\eta_i)\mathscr{C}$$
$$D_{cl}(\eta_i)=D_{11}(\eta_i)+\mathscr{D}_{12}\Omega(\eta_i)\mathscr{D}_{21} \tag{14}$$

and

$$A_o = \begin{bmatrix} A_i^a(\eta_i) & 0 \\ 0 & 0_{k \times k} \end{bmatrix}, B_o = \begin{bmatrix} B_1^a \\ 0 \end{bmatrix},$$

$$C_o = [C_{1,i}^a \ 0], \quad \mathscr{B} = \begin{bmatrix} 0 & B_i^a \\ I_k & 0 \end{bmatrix} \quad (15)$$

$$\mathscr{C} = \begin{bmatrix} 0 & I_k \\ C^a & 0 \end{bmatrix}, \mathscr{D}_{12} = [0 \ D_{12}], \mathscr{D}_{21} = \begin{bmatrix} 0 \\ 0 \end{bmatrix}$$

The assumptions on the plant are:

- The pairs (A_i^a, B_i^a) and (A_i^a, C^a), are quadratically stabilizable and quadratically detectable respectively.

Under the posed assumptions of the LPV-plant, there exists an LPV-controller [36] guaranteeing Quadratic H_∞ performance $\leq \gamma$ for all state vector trajectories $\eta(t) \in [\eta^{\min}, \eta^{\max}] = \mathrm{Co}\{\eta_i^o, i = 1, \ldots, M\}$ if and only if there exist two symmetric matrices R, S satisfying the system of LMIs:

$$\hat{N}_R^T \begin{bmatrix} A_i^a R + R(A_i^a)^T & R(C_{1,i}^a)^T & B_1^a \\ C_{1,i}^a R & -\gamma I & D_{11} \\ (B_1^a)^T & D_{11}^T & -\gamma I \end{bmatrix} \hat{N}_R < 0$$

$$\hat{N}_S^T \begin{bmatrix} (A_i^a)^T S + S A_i^a & S B_i^a & (C_{1,i}^a)^T \\ (B_1^a)^T S & -\gamma I & D_{11}^T \\ C_{1,i}^a & D_{11} & -\gamma I \end{bmatrix} \hat{N}_S < 0$$

$$\begin{bmatrix} R & I \\ I & S \end{bmatrix} \geq 0$$

where

$$\hat{N}_R = \begin{bmatrix} N_R & 0 \\ 0 & I \end{bmatrix}, \quad \hat{N}_S = \begin{bmatrix} N_S & 0 \\ 0 & I \end{bmatrix}$$

and N_R and N_S are the orthonormal bases of the null spac $[(B_i^a)^T, D_{12}^T]$ and $[C^a, D_{21}]$ respectively. Moreover there k-th order LPV controllers solving the same LMI proble and only if R, S would also satisfy the rank constraint

$$\mathrm{rank}(I - RS) \leq k. \quad (20)$$

After the computation of any feasible solution of R and S matrices the invertible matrices Θ and Ψ can be computed via a SVD as:

$$\Theta \Psi^T = I - RS. \quad (21)$$

Having computed Θ and Ψ the matrix X_{cl} is formed as:

$$X_{cl} = \begin{bmatrix} I_{2 \times 2} & S \\ 0_{2 \times 2} & \Psi^T \end{bmatrix} \begin{bmatrix} R & I_{2 \times 2} \\ \Theta^T & 0_{2 \times 2} \end{bmatrix}^{-1}. \quad (22)$$

Given the matrix X_{cl} a possible choice of vertex controller:

$$\Omega_i = \begin{bmatrix} A_c(\eta_i) & B_c(\eta_i) \\ C_c(\eta_i) & D_c(\eta_i) \end{bmatrix} \quad (23)$$

is any feasible solution of the LMI problem:

$$\begin{bmatrix} A_{cl}^T(\eta_i) X_{cl} + X_{cl} A_{cl}(\eta_i) & X_{cl} B_{cl}^T(\eta_i) & C_{cl}(\eta_i)^T \\ B_{cl}(\eta_i) X_{cl} & -\gamma I & 0 \\ C_{cl}(\eta_i) & 0 & -\gamma I \end{bmatrix} < 0. \quad (24)$$

IV. SIMULATION RESULTS

Simulation studies were carried on a EmA's non–linear model [17]. The parameters of the system unless otherwise stated are equal to those presented in the following Table.

parameter (Unit)	Description	Value
A (m^2)	Area of the plates	10×10^{-8}
ℓ (m)	Plate Length	100×10^{-6}
μ $(kg \ m/sec^2)$	Viscosity Coefficient	18.5×10^{-6}
ρ (kg/m^3)	Density	1.155
ε $(coul^2/Nm^2)$	Dielectric constant of the air	8.85×10^{-12}
P_a (N/m^2)	Ambient Pressure	10^5
k (N/m)	Stiffness of the spring	0.816

Figure 4 shows the relationship between the magnitude frequency responses of the "linearized" and the approximated 2nd-order linearized subsystems, presented in Equations (7), (9) respectively parameterized with respect to η_i^o. As observed from the plots the systems' frequency representations are very close considering critical issue points (i.e. system's dc-gain, resonant frequency, stability issues etc).
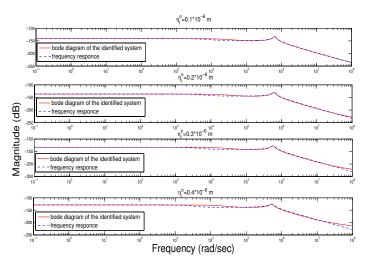

Fig. 4. Frequency magnitude comparison between actual and aggregated (2nd-order) linearized EmA-systems.

The plate's gap is constrained within $\eta \in [0.1, 2)\,\mu m$ resulting in an operating regime below the well-known bifurcation point [13], [17]. Figure 5 presents the bifurcation points of the system for different values of the frequency ω. In the presented Figure the x-axis corresponds to η, the y-axis corresponds to the value of the frequency ω and the z-axis corresponds to the value of the voltage as derived from Equation (6). The extrema of the graphs presented in this figure are equal to the bifurcation points of the system. These are the points where the behavior of the system changes from stable to unstable and vice versa. These points can easily be found by setting the derivative of $\frac{\partial U_o}{\partial \eta}$ of the expression in equation (6) equal to zero. It should be noted that in the absence of the squeezed thin film damping effect, there is a single bifurcation point at $\frac{\eta}{\eta^{\max}} = \frac{1}{3}$.

Since the operating regime is below the well-known bifurcation point [13], [17], the linearized systems are stable, as expected and verified from the Nyquist plots of these systems shown in Figure 6.

In the following Figures 7, 8 the 3-D frequency plots are presented for the approximated systems for different values
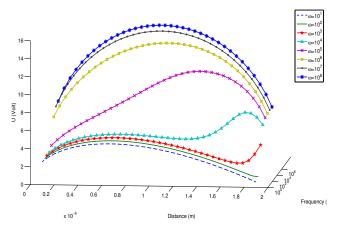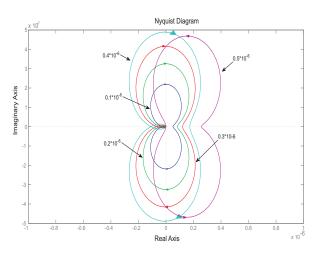
Fig. 5. EmA's bifurcation points for different ω

Fig. 6. Nyquist diagrams for linearized EmA-systems parametrized for different operating points

of $\eta^{\max}$ ($\eta^{\max} = 0.2$, $2\mu m$) between the two plates. In these Figures the x-axis represents the frequency in (rad/sec), the y-axis represents the the values of different η_i^o in (m), the z-axis represents the magnitude of the transfer functions in (dB).

As it is observed from the plots the gap between the plates of the EmA has a significant role in the system's behavior. In all plots, there is a variation in the 2nd-order system's natural frequency as η_i^o changes. In general the natural frequency monotonically increases with η_i^o. The reduction of the damping ($\zeta \simeq 0.05$) is crucial in EmAs with tiny gaps ($\simeq 0.2\mu$m) since the squeezed air cannot provide sufficient reacting force.

The system's response to a reference periodic square signal of period T_s

$$\eta^\Gamma = \begin{cases} \eta^{\Gamma,\max} & t \in [0, T_s/2) \\ \eta^{\Gamma,\min} & t \in [T_s/2, T_s) \end{cases} \qquad (25)$$

The reference signal is analyzed in its Fourier series, and R_a-terms are kept in the sum as:

$$\eta^\Gamma = \sum_{i=\text{odd}}^{Ra} R_i sin\left(\frac{2\pi}{iT_s}t + \varphi_i\right) \qquad (26)$$
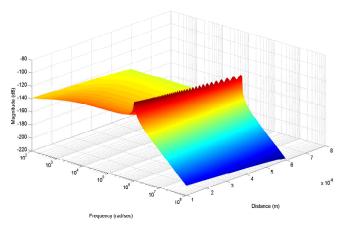

Fig. 7. Magnitude frequency diagrams for different η_i^o and $\eta^{\max} = 0.2 \times 10^{-6}$ m
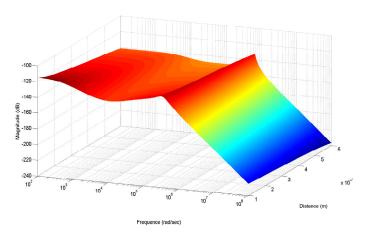

Fig. 8. Magnitude frequency diagrams for different η_i^o and $\eta^{\max} = 2 \times 10^{-6}$m

In Figure 9, the EmA-system's response for R_a=7, $\eta^{\Gamma,\max} = 0.25\mu m$, $\eta^{\Gamma,\min} = 0.15\mu m$ is presented. The measurements are corrupted with noise resulting in a SNR=20dB. The oscillatory nature of the response is primarily caused by the truncation of the Fourier series.

V. CONCLUSIONS

In this article a Gain scheduling H_∞ controller tuned via the theory of LMIs has been designed for an approximated model of an EmA with squeeze film gas film damping effect. The controller is designed at various operating points and smoothly changes its values as the upper plate of the EmA is moving. The overall control scheme is applied on the EmA's non linear model in order to test its efficacy.
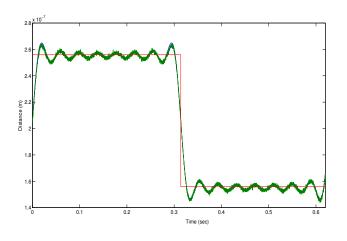
Fig. 9. Nonlinear System's output

VI. ACKNOWLEDGMENTS

REFERENCES

[1] J. Judy. Microelectromechanical systems (MEMS): fabrication, design and applications, *Smart materials and Structures* 10. pp. 1115–1134, 2001.

[2] M.Vagia, G. Nikolakopoulos and A. Tzes Intelligent Robust Controller Design for a micro–Actuator, *Journal of Intelligent and Robotic Systems* 47. pp. 299-315, 2006.

[3] B. Ilic, Y. Yang, HG Crainghead Virus detecting using nanoelectromechanical devices, *Appl Physic Letters* vol. 85, pp. 2604-2606, 2004.

[4] A. K. Pandey, R. Pratap, F.S. Chau Effect of Pressure on Fluid Damping in MEMS Torsional Resonators with Flow Ranging from Continuum to Molecular Regime *Journal of Experimental Mechanics*, vol. 48, pp.91-106, 2008.

[5] A. Agarwal, S. Sridharamurthy, D. Beebe Programmable autonomous micromixers and micropumps, *IEEE Journal of Microelectromechanical Systems* 14. pp. 1409-1421, 2005.

[6] C. H. Chu, W. P. Shih, S. Y. Chung, H. C. Tsai, T. K. Shing and P. Z. Chang. A low actuation voltage electrostatic actuator for RF MEMS switch applications, J. Micromech. Microeng 17. pp. 1649-1656, 2007.

[7] A. Menciassi, A. Eisinberg, I. Izzo and P. Dario From "macro" to "micro" Manipulation: Models and Experiments, *IEEE-ASME Transactions on Mechatronics* 9. pp. 311–320, 2004.

[8] M. S. C. Lu and G. Fedder. Position Control of Parallel-Plate Microactuators for Probe-Based Data Storage, *Journal of microelectromechanical Systems* 13. pp. 759–769, 2004.

[9] A. Ketsdever, R. Lee and T. Lilly Performance testing of a microfabricated propulsion system for nanosatellite applications, *Journal of Micromechanics and Microengineering*. 15. pp. 2254–2263, 2005.

[10] J.B. Starr Squeeze film Damping in solid-state accelerometers, *Solid-State Sensor and Actuator Workshop 4th Technical Digest., IEEE*, pp.44-47, 1990.

[11] C.C. Hwang, R. F. Fung, R.F. Yang, C.I. Weng and W.L. Li A new modified Reynolds equation for ultrathin film gas lubrication , *IEEE Transactions on Magnetics*, 32, pp. 344-347, 1996.

[12] K.M Chang, S.C Lee and S.H. Li Squeeze film damping effect on a MEMS torsion mirror, *Journal of Micromechanics and Microengineering*, 12, pp. 556-561, 2002.

[13] M.Vagia and A. Tzes, Robust PID-control design for an electrostatic micromechanical actuator with structured uncertainty, *In IET journal of Control theory and Applications* .vol. 2, pp. 365-373, 2008

[14] D. Yan and A. Lal The squeeze film damping effect of perforated microscanners: modeling and characterization, *Smart Materials and Structures* 15. pp.480-484, 2006.

[15] M. Bo, H. Yang, Squeeze film air damping in MEMS, *Sensors and Actuators A* 136. pp. 3-27, 2007.

[16] X. Rottenberg, S. Brebels, P. Ekkels, P. Czarnecki, P. Nolmans, R. P. Mertens, B. Nauwelaers, R. Puers, I. De Wolf, W. De Raedt and H. A. C. Tilmans An electrostatic fringing-field actuator (EFFA): application towards a low-complexity thin-film RF-MEMS technology, *J. Micromech. Microeng* 17. pp. 204-210, 2007.

[17] M.Vagia and A. Tzes Robust PID Controller Design for a micro-Actuator with Squeezed Gas Film Damping Effects, *In the Proceedings of the IFAC World Congress*, 2008.

[18] J. Shamma and M. Athans, Gain scheduling: Potential Hazards and Posible Remendies, *IEEE Control Systems Magazine*,vol 12, pp. 101-107.

[19] G. Balas Linear Parameter Varying Control and its applications to a turbofan Engine, *International Journal of Robust and Nonlinear Control*,vol 12, pp.763-796.

[20] S. Zhou, B. Zhang and W.X. Zheng, Gain scheduled $H\infty$ filtering of parameter-varying systems, *International Journal of Robust and nonlinear control*,vol 6, pp. 397-411.

[21] S. Hong, V. Varadan and V. Varadan. Implementation of coupled mode optimal structural vibration control using approximated eigenfunctions, *Smart Material Structures* 7. pp. 63–71, 1998.

[22] M. Zarubinskaya and W. Horssen On the free vibrations of a rectangular plate with two opposite sides simply supported and the other sides attached to linear springs, *Journal of Sound and Vibration* 278. pp. 1081–1093, 2003.

[23] D. Maithripala, J. Berg and P. Dayawansa Control of an Electrostatic Microelectromechanical System Using Static and Dynamic Output Feedback, *ASME's Journal of Dynamic Systems, Measurement, and Control* 127. pp. 443–450, 2003.

[24] A. Rocha, E. Cretu and R. F. Wolffenbuttel Using dynamic voltage drive in a parallel-plate electrostatic actuator for full-gap travel range and positioning, *Journal of Microelectromechanical Systems* 15. pp. 69–83, 2006.

[25] E. Chen and R.W. Dutton. Electrostatic Micromechanical Actuator with extended range of travel, *Journal of microelectromechanical Systems* 9. pp. 321–328, 2000.

[26] W. A. Gross, L. A. Matsch, V. Castelli, A. Eshel, J. H. Vohr, M. Wildman *Fluid Film Lubrication*, John Willey and Sons, 1980.

[27] W. L. Li Squeeze filmEffects on Dynamic performance of MEMS μ-mirrors- consideration of gas rarefaction and surface roughness, *Journal of Microsystems Technlogy*, vol. 14, pp. 315-324, 2008.

[28] J.J. Blench. On isothermal Squeeze Films, *Journal of Lubrication Technology*. 105. pp.615-620, 1983.

[29] T. Veijola Compact models for squeezed-film dampers with inertial effects, *In the proceedings of the Conference of Design, Test, Integration and Packaging of MEMS/MOEMS*,DTIP, Montreux, Switcherland May, 2004.

[30] E. Westby and T.A. Fjeldy Dynamical Equivalent- Circuit Modelling of MEMS with Sqeezed Gas Film Damping, *Physical Scripta* 101. pp.192-195, 2002.

[31] S. Vemuri, G.Fedder and T. Mukheree Low-order Squeeze film model for simulation of MEMS devices. *In the Proceedings of the International Conference on Modeling and Simulation of Microsystems* San Diego, USA, pp.205 - 208, March 2000.

[32] T. Veijola, H. Kuisma, J. Lahdenpera and T. Ryhanen Equivalent-circuit Model of squeezed gas film in a silicon accelerometer, *Sensors and Actuators* A. 48. pp.239-248,1995.

[33] P. Apkarian, P. Gahinet A convex characterization of Gain-Scheduled H_∞ controllers, *IEEE Trans. Automatic Control,* vol. 40, no. 5, pp. 853-864, 1995 .

[34] P. Apkarian and P. Gahinet and G. Becker Self-Scheduled H_∞ Control of Linear Parameter-Varying Systems: A Design Example *Automatica*, vol. 31, no. 9, pp. 1251-1261, 1995.

[35] A.Packard, Gain Scheduling via Linear Fractional Transformation, Systems and Control Leters, vol. 22,pp.79-92.

[36] G. Becker and A. Packard Robust Performance of Linear Parametrically Varying Systems Dependent Linear Feedback, *Systems and Control Letters*, vol.23, (1994), pp.205-215.